# Expanding the molecular-ruler process through vapor deposition of hexadecanethiol

Alexandra M. Patron<sup>1</sup>, Timothy S. Hooker<sup>2</sup>, Daniel F. Santavicca<sup>2</sup>, Corey P. Causey<sup>\*1,§</sup> and Thomas J. Mullen<sup>\*1,¶</sup>

Letter

Address:

<sup>1</sup>Department of Chemistry, University of North Florida, Jacksonville, FL 32224, USA and <sup>2</sup>Department of Physics, University of North Florida, Jacksonville, FL 32224, USA

**Email** 

Corey P. Causey\* - corey.causey@unf.edu; Thomas J. Mullen\* - tj.mullen@unf.edu

\* Corresponding author

§ Phone: +1 904 620 2098; Fax: +1 904 620 3535 ¶ Phone: +1 904 620 1377; Fax: +1 904 620 3535

Keywords:

hybrid nanolithography; metal-ligated multilayer; molecular ruler; self-assembled monolayers; vapor-phase deposition

Beilstein J. Nanotechnol. **2017**, 8, 2339–2344. doi:10.3762/bjnano.8.233

Received: 30 June 2017 Accepted: 09 October 2017 Published: 07 November 2017

This article is part of the Thematic Series "Nanoscale patterning and

characterization".

Guest Editor: S. A. Claridge

© 2017 Patron et al.; licensee Beilstein-Institut. License and terms: see end of document.

#### Abstract

The development of methods to produce nanoscale features with tailored chemical functionalities is fundamental for applications such as nanoelectronics and sensor fabrication. The molecular-ruler process shows great utility for this purpose as it combines top-down lithography for the creation of complex architectures over large areas in conjunction with molecular self-assembly, which enables precise control over the physical and chemical properties of small local features. The molecular-ruler process, which most commonly uses mercaptoalkanoic acids and metal ions to generate metal-ligated multilayers, can be employed to produce registered nanogaps between metal features. Expansion of this methodology to include molecules with other chemical functionalities could greatly expand the overall versatility, and thus the utility, of this process. Herein, we explore the use of alkanethiol molecules as the terminating layer of metal-ligated multilayers. During this study, it was discovered that the solution deposition of alkanethiol molecules resulted in low overall surface coverage with features that varied in height. Because features with varied heights are not conducive to the production of uniform nanogaps via the molecular-ruler process, the vapor-phase deposition of alkanethiol molecules was explored. Unlike the solution-phase deposition, alkanethiol islands produced by vapor-phase deposition exhibited markedly higher surface coverages of uniform heights. To illustrate the applicability of this method, metal-ligated multilayers, both with and without an alkanethiol capping layer, were utilized to create nanogaps between Au features using the molecular-ruler process.

## **Findings**

In a time when many technological advances are driven by the miniaturization of fabrication methods, much effort has been placed on the development of novel methods to produce nanoscale features with chemical functionalities that go beyond traditional semiconductors [1-3]. Recent advances in the field allow for the fabrication of molecular-scale features into surfaces that template the assembly and growth of metals, polymers, biomolecules, and cellular structures [3-11]. In addition, these surface assemblies have been utilized as molecular-scale resists for lithography [12,13]. One promising strategy for such fabrication utilizes top-down lithography to create complex architectures over large areas in conjunction with molecular self-assembly, which enables precise control over the physical and chemical properties of the small features [1,2]. The molecular-ruler process is a notable example of this hybrid approach as it couples conventional patterning methods with molecular selfassembly [14].

The molecular-ruler process can be employed to form nanogaps between registered metal surface features that have been generated using conventional lithographic techniques such as photolithography or electron-beam lithography (Figure 1) [14-24]. In short, a metal structure that has been patterned on a nonmetal substrate (e.g., Si) using conventional lithography is subsequently covered by a metal-ligated multilayer through the iterative deposition of bifunctional organic molecules and metal ions. Note that the use of a thiol as one of the two functionalities ensures that deposition and growth of the multilayer only occurs on the surface of the metal, not the exposed substrate. By using molecules of discrete length, the thickness of the multilayer can be precisely controlled through the number of deposition steps. Once the desired thickness has been achieved, a second metal deposition is used to cover the entire sample of the substrate, including the exposed substrate and the surface of the multilayer. Following this second metal deposition, a chemical lift-off removes the labile multilayer, thus exposing the initial metal feature and the portion of the substrate that was masked by the multilayer, yielding a nanogap between the two metal surfaces. The size of this gap is defined by the thickness of the multilayer. Utilization of the molecular-ruler process in this way provides a general and widely applicable method to fabricate registered, nanometer-scale features for potential applications including nanoelectronics, molecular-scale junctions, and electrochemical sensors [17,18,20,21,25,26].

Although mercaptoalkanoic acid molecules, such as 16-mercaptohexadecanoic acid (MHDA), are the most widely studied molecules used in the molecular-ruler process, this method is inherently versatile through the use of molecules with alternate functionalities [27-31]. Towards this end, we set out to explore the

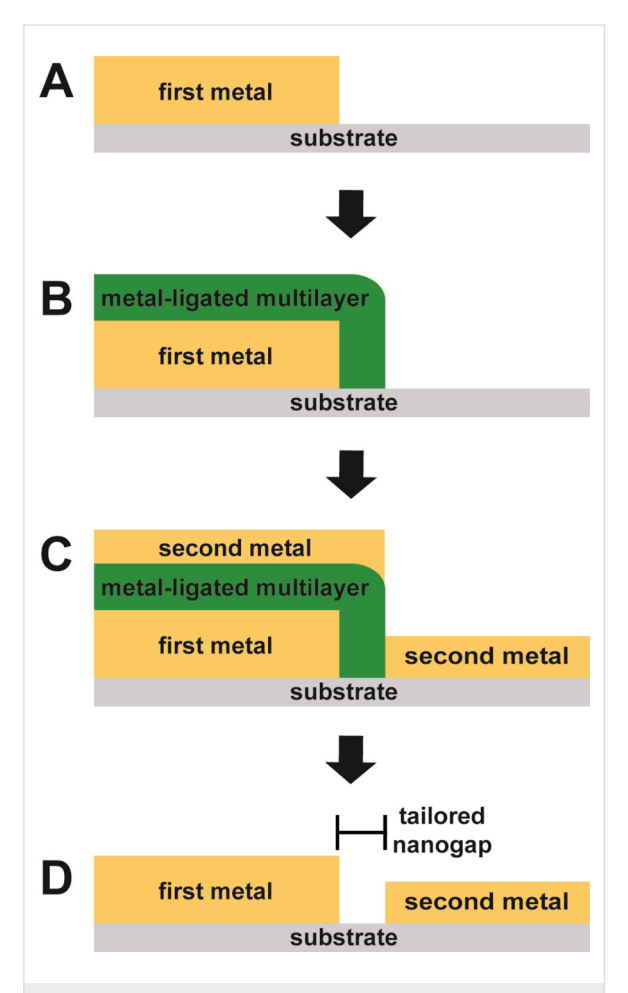
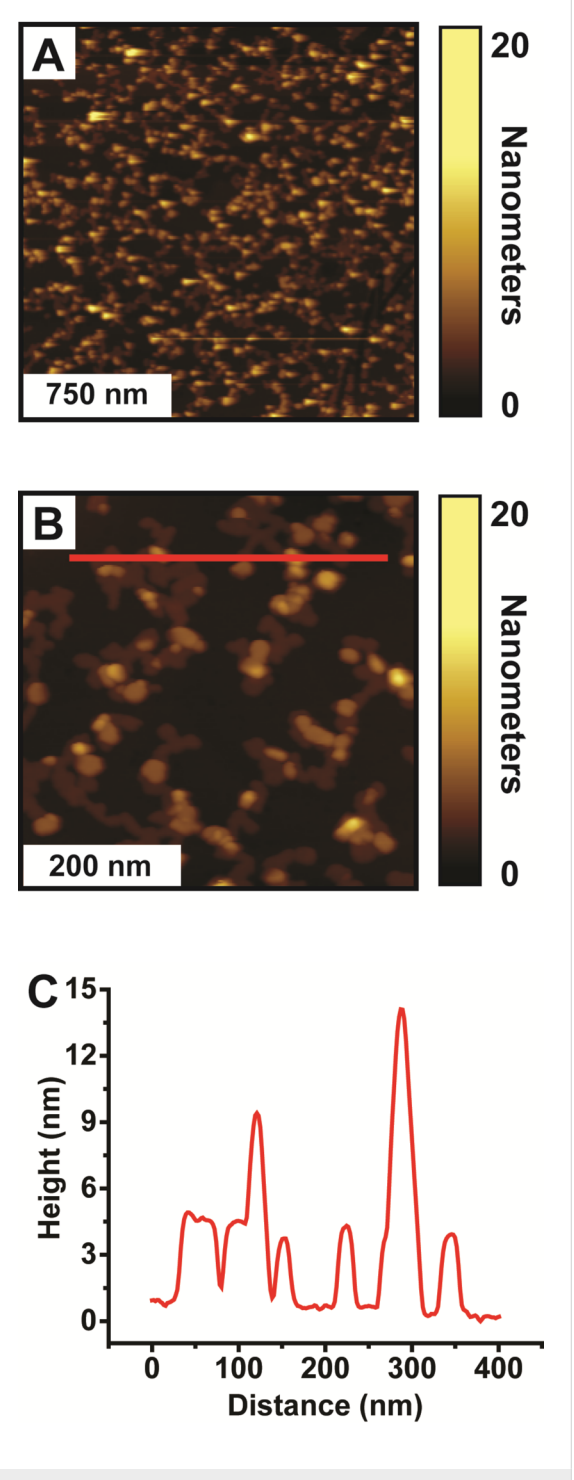


Figure 1: Key steps for the molecular-ruler process. (A) A metal is patterned on a substrate via conventional lithography. (B) A molecular-ruler, consisting of alternating layers of thiol molecules and metal ions, is created only on the first metal structure. (C) A second metal is deposited. (D) Upon removal of the molecular-ruler and the second metal on top of the multilayer via a chemical lift-off, a tailored nanogap is generated with a width that corresponds to the thickness of the multilayer.

use of an alkanethiol, specifically 1-hexadecanethiol (C16), as the terminating layer of a metal-ligated multilayer. This molecule was selected as it is commonly used to produce well-ordered self-assembled monolayers, has a relatively well understood terminal functionality (e.g., a methyl group), and enables direct comparison of thickness to MHDA molecules. Figures 2A and 2B show representative 2  $\mu m \times 2 \mu m$  and 500 nm  $\times$  500 nm atomic force microscopy (AFM) images of a Cu-ligated MHDA-C16 bilayer formed from the solution deposition of MHDA for 18 h, Cu(ClO<sub>4</sub>)<sub>2</sub>·6H<sub>2</sub>O for 5 min, and C16 for 1 h. Figure 2C displays a representative cursor profile across several islands as indicated by the red line in Figure 2B. Although C16 is very similar in structure to MHDA, the solution

deposition of C16 results in structures that exhibit islands of various apparent heights, ranging from 3.4 to 24.8 nm, with relatively low surface coverages (38.2  $\pm$  3.3%). This is in contrast to Cu-ligated MHDA bilayers, which exhibit islands of uniform height (ca. 2.2 nm) and have surface coverages of about 50% [27-29,32]. The C16 islands of the Cu-ligated MHDA-C16 bilayers are observed across the Au{111} substrate and are attributed to C16 molecules bound to a MHDA monolayer via cupric ions. The morphology of these islands is consistent with previous AFM topographic images of solution-deposited Cu-ligated MHDA-C16 bilayers [27]. This surface morphology results in a RMS roughness of  $3.2 \pm 0.5$  nm, which is considerably larger than previously reported RMS roughnesses for MHDA monolayers (ca. 0.1 nm) and MHDA bilayers (1.0 nm) [32]. Similar morphology and slightly higher coverages of the C16 islands are observed when C16 is deposited from solution at 80 °C (Figure S1, Supporting Information File 1). Given the roughness and variations in the surface morphology of the Cu-ligated MHDA-C16 bilayers, it seems that the solution deposition of C16 is not suitable for use in the molecular-ruler process, and specifically for producing nanogaps with reproducible uniformity.

To overcome this limitation, the vapor deposition of C16 is explored. Interestingly, when C16 is deposited from the vapor phase onto MHDA monolayers to produce Cu-ligated MHDA-C16 bilayers, protruding islands with uniform thickness are observed across the Au{111} substrate (Figure 3). Figure 3A and Figure 3B show representative 2  $\mu m \times 2 \mu m$  and 500 nm × 500 nm AFM images of a Cu-ligated MHDA-C16 bilayer formed from the solution deposition of MHDA for 18 h and Cu(ClO<sub>4</sub>)<sub>2</sub>·6H<sub>2</sub>O for 5 min followed by vapor deposition of C16 for 1 h at 80 °C. Figure 3C displays a representative cursor profile across several islands as indicated by the red line in Figure 3B. The apparent height of these protruding islands  $(3.6 \pm 0.2 \text{ nm})$  is consistent with the least-protruding C16 islands of the Cu-ligated MHDA-C16 bilayers formed via solution deposition. Protruding islands of greater thicknesses are not observed. The surface morphology of the Cu-ligated MHDA-C16 bilayer formed via vapor deposition results in a RMS roughness of  $1.3 \pm 0.1$  nm, which is smaller than a Cu-ligated MHDA-C16 bilayer formed via solution deposition. Further, the surface coverage of these C16 islands (69.9  $\pm$  1.8%) is considerably higher than the C16 surface coverage for the MHDA-C16 bilayer formed via solution deposition. Given the increase in surface coverage coupled with the marked decrease in roughness, this method is far more amendable to our goal of nanogap formation. It should be noted that thickness of the C16 islands is roughly twice as thick as predicted, which has been observed in other studies [27,33,34]. Although the explanation of this height discrepancy it not completely clear, it is conceivable that



**Figure 2:** Cu-ligated MHDA-C16 bilayer formed from solution-phase deposition of C16. Representative (A)  $2 \mu m \times 2 \mu m$  and (B)  $500 \text{ nm} \times 500 \text{ nm}$  AFM images of a Cu-ligated MHDA-C16 bilayer formed from the solution deposition of MHDA for 18 h,  $\text{Cu}(\text{ClO}_4)_2 \cdot 6\text{H}_2\text{O}$  for 5 min, and C16 for 1 h. (C) Corresponding cursor profile across the C16 islands.

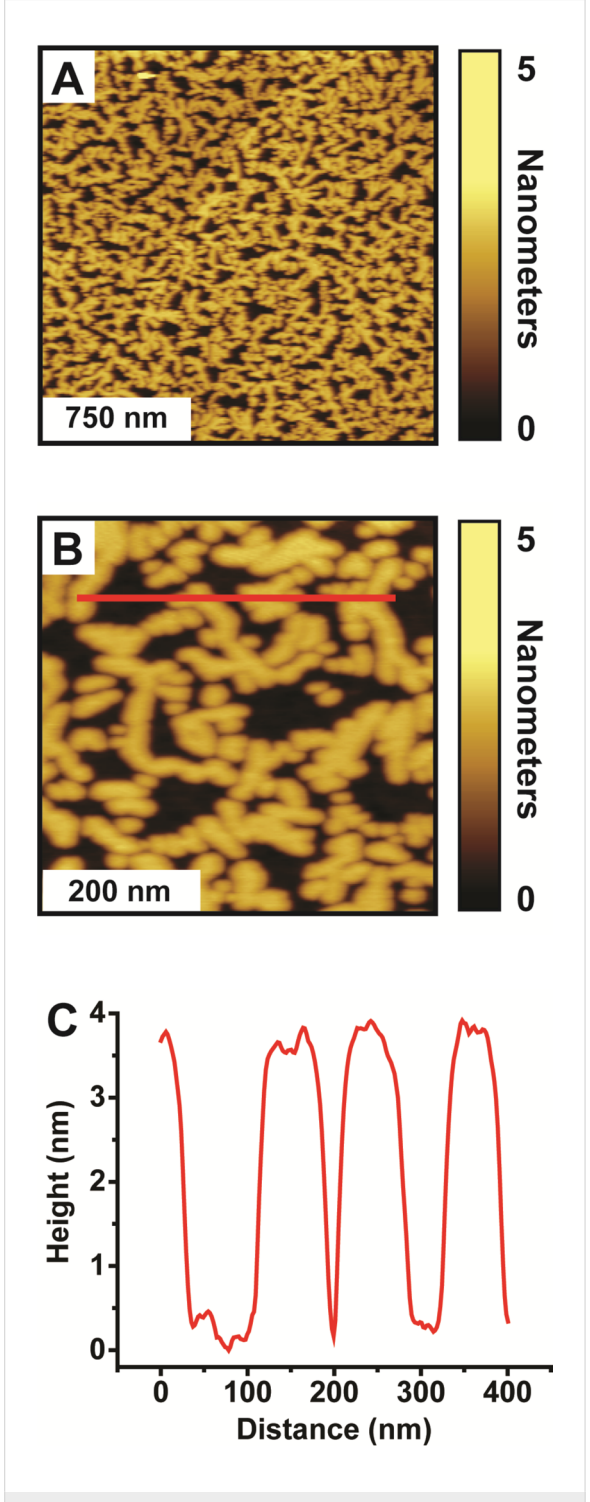


**Figure 3:** Cu-ligated MHDA-C16 bilayer formed from vapor-phase deposition of C16. Representative (A) 2  $\mu$ m × 2  $\mu$ m and (B) 500 nm × 500 nm AFM images of a of a Cu-ligated MHDA-C16 bilayer formed from the solution deposition of MHDA for 18 h and Cu(ClO<sub>4</sub>)<sub>2</sub>·6H<sub>2</sub>O for 5 min and the vapor deposition of C16 for 1 h at 80 °C. (C) Corresponding cursor profile across the C16 islands.

the doubling in height results from disulfides that are intercalated into the hydrocarbon tails of the Cu-ligated C16 molecules.

To illustrate the applicability of the vapor-phase deposition of C16 in the molecular ruler process, Cu-ligated MHDA multilayers with and without a C16 capping layer are utilized to create nanogaps via the molecular-ruler process. Figure 4A shows a scanning electron microscope (SEM) image of the resulting nanogaps from nine iterations of the solution deposition of MHDA and Cu(ClO<sub>4</sub>)<sub>2</sub>·6H<sub>2</sub>O followed by the solution deposition of MHDA for 1 h. The higher-intensity region corresponds to the first Au deposition (100 nm thick) before multilayer growth, and the lower-intensity region corresponds to the second Au deposition (30 nm thick) after multilayer growth. The lowest-intensity region between the two Au regions corresponds to the nanogap where the Si substrate is exposed. This nanogap measures  $26.0 \pm 4.3$  nm and is consistent with the

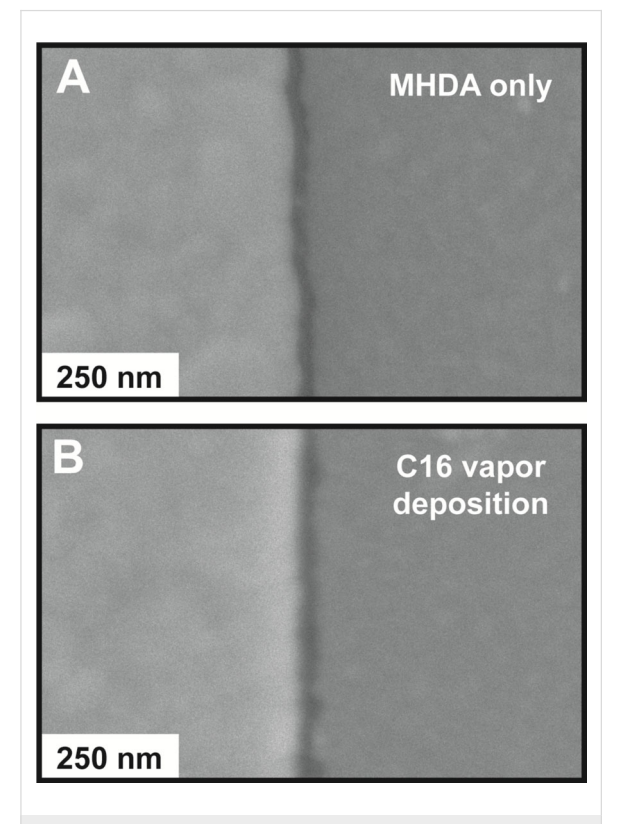


**Figure 4:** Nanogaps from MHDA only and MHDA with vapor-phase deposition of C16. (A) A representative SEM image of a nanogap fabricated from nine iterations of the solution deposition of MHDA and  $\text{Cu}(\text{ClO}_4)_2\text{-}6\text{H}_2\text{O}$  followed by the solution deposition of MHDA. (B) A representative SEM image of a nanogap from ten iterations of the solution deposition of MHDA and  $\text{Cu}(\text{ClO}_4)_2\text{-}6\text{H}_2\text{O}$  followed by the vapor deposition of C16. In both SEM images, the initial Au structure (100 nm thick) is on the left, and the second layer of Au (30 nm thick) is on the right.

thickness of the Cu-ligated MHDA decalayer measured via spectroscopic ellipsometry ( $24.8 \pm 0.1$  nm) and the thickness of Cu-ligated MHDA decalayers from previous studies [28].

Figure 4B shows an SEM image of the resulting nanogaps from ten iterations of the solution deposition of MHDA and Cu(ClO<sub>4</sub>)<sub>2</sub>·6H<sub>2</sub>O followed by the vapor deposition of C16 at 80 °C for 1 h. Similar higher and lower intensity regions are observed and correspond to the first and second Au deposition steps. The nanogap between the two Au regions measures  $31.0 \pm 9.4$  nm, which is both larger and exhibits greater variability than the nanogap without the C16 capping layer. The width is consistent with the thickness of a Cu-ligated MHDA decalayer with the C16 capping ( $31.0 \pm 1.0$  nm) measured via spectroscopic ellipsometry.

The standard deviations of the nanogap widths, thus the quality of the nanogaps, result from the morphologies of the Cu-ligated multilayers of MHDA only and MHDA with vapor-phase deposition of C16 (Figure S2, Supporting Information File 1). The surface morphology of the 10-layer Cu-ligated MHDA multilayer with a C16 capping layer appears rougher with protruding islands with larger cross sections when compared to the 10-layer Cu-ligated MHDA multilayer without a C16 capping layer. Although the nanogaps produced from the Cu-ligated MHDA multilayer with a C16 capping layer have somewhat larger standard deviation, these nanogaps illustrate that alternate chemical functionalities can be utilized in the molecular-ruler process.

In conclusion, Cu-ligated MHDA-C16 bilayers formed from the solution and vapor deposition of C16 have been characterized with AFM revealing varied surface morphologies. The solution deposition of C16 results in structures that exhibit protruding islands of varying heights with relatively low surface coverages. These results agree with previous AFM topographic images of solution deposited Cu-ligated MHDA-C16 bilayers [27]. The vapor deposition of C16 produces protruding islands with uniform apparent heights and relatively high surface coverages. Given the increase in surface coverage coupled with the marked decrease in roughness for C16 islands formed from the vaporphase deposition, Cu-ligated MHDA multilayers, without and with a vapor-phase deposited C16 capping layer, were utilized to create nanogaps between Au features using the molecularruler process. Although the quality of the nanogaps formed using the vapor-phase deposited C16 capping layer is diminished (i.e., the standard deviation is larger) when compared to MHDA multilayers, this is a minor tradeoff considering this approach enables the utilization of molecules with alternate functionalities beyond carboxylic acid into the molecular-ruler process. Efforts to explore the underling mechanism for the increased thickness of the C16 islands and to apply this strategy to other bifunctional thiol molecules are ongoing.

## Supporting Information

Supporting Information features additional AFM data and experimental details.

#### Supporting Information File 1

Additional experimental data.

[http://www.beilstein-journals.org/bjnano/content/supplementary/2190-4286-8-233-S1.pdf]

## Acknowledgements

This work was supported by the National Science Foundation (CMMI-1536528) and a UNF Academic Affairs Faculty Development Scholarship Grant. We thank Mr. Jackson Neuman, Mr. Joel Serrano, Mr. Cameron Kilgore, Mr. Michael VanMiddlesworth, Prof. Josh Melko, and Prof. Tao Ye for helpful and insightful discussions and the UNF Materials Science and Engineering Research Facility (MSERF) for the use of equipment.

#### References

- Mullen, T. J.; Srinivasan, C.; Shuster, M. J.; Horn, M. W.; Andrews, A. M.; Weiss, P. S. J. Nanopart. Res. 2008, 10, 1231–1240. doi:10.1007/s11051-008-9395-v
- Saavedra, H. M.; Mullen, T. J.; Zhang, P.; Dewey, D. C.; Claridge, S. A.; Weiss, P. S. Rep. Prog. Phys. 2010, 73, 036501. doi:10.1088/0034-4885/73/3/036501
- Smith, R. K.; Lewis, P. A.; Weiss, P. S. Prog. Surf. Sci. 2004, 75, 1–68. doi:10.1016/j.progsurf.2003.12.001
- Whitesides, G. M.; Ostuni, E.; Takayama, S.; Jiang, X. Y.; Ingber, D. E. Annu. Rev. Biomed. Eng. 2001, 3, 335–373. doi:10.1146/annurev.bioeng.3.1.335
- Kasemo, B. Surf. Sci. 2002, 500, 656–677. doi:10.1016/S0039-6028(01)01809-X
- Mantooth, B. A.; Weiss, P. S. Proc. IEEE 2003, 91, 1785–1802. doi:10.1109/JPROC.2003.818320
- Tirrell, M.; Kokkoli, E.; Biesalski, M. Surf. Sci. 2002, 500, 61–83. doi:10.1016/S0039-6028(01)01548-5
- Pathem, B. K.; Claridge, S. A.; Zheng, Y. B.; Weiss, P. S. *Annu. Rev. Phys. Chem.* 2013, 64, 605–630. doi:10.1146/annurev-physchem-040412-110045
- Alivisatos, A. P.; Andrews, A. M.; Boyden, E. S.; Chun, M.; Church, G. M.; Deisseroth, K.; Donoghue, J. P.; Fraser, S. E.; Lippincott-Schwartz, J.; Looger, L. L.; Masmanidis, S.; McEuen, P. L.; Nurmikko, A. V.; Park, H.; Peterka, D. S.; Reid, C.; Roukes, M. L.; Scherer, A.; Schnitzer, M.; Sejnowski, T. J.; Shepard, K. L.; Tsao, D.; Turrigiano, G.; Weiss, P. S.; Xu, C.; Yuste, R.; Zhuang, X. W. ACS Nano 2013, 7, 1850–1866. doi:10.1021/nn4012847
- Gates, B. D.; Xu, Q. B.; Stewart, M.; Ryan, D.; Willson, C. G.; Whitesides, G. M. Chem. Rev. 2005, 105, 1171–1196. doi:10.1021/cr0300760

- 11. Weiss, P. S. Acc. Chem. Res. **2008**, *41*, 1772–1781. doi:10.1021/ar8001443
- Johnson, S.; Evans, D.; Davies, A. G.; Linfield, E. H.; Wälti, C. Nanotechnology 2009, 20, 155304. doi:10.1088/0957-4484/20/15/155304
- 13. Xia, Y. N.; Rogers, J. A.; Paul, K. E.; Whitesides, G. M. *Chem. Rev.* **1999**, 99, 1823–1848. doi:10.1021/cr980002q
- Hatzor, A.; Weiss, P. S. Science 2001, 291, 1019–1020. doi:10.1126/science.1057553
- Anderson, M. E.; Smith, R. K.; Donhauser, Z. J.; Hatzor, A.;
   Lewis, P. A.; Tan, L. P.; Tanaka, H.; Horn, M. W.; Weiss, P. S.
   J. Vac. Sci. Technol., B 2002, 20, 2739–2744. doi:10.1116/1.1515301
- Anderson, M. E.; Srinivasan, C.; Hohman, J. N.; Carter, E. M.;
   Horn, M. W.; Weiss, P. S. Adv. Mater. 2006, 18, 3258–3260.
   doi:10.1002/adma.200601258
- Anderson, M. E.; Srinivasan, C.; Jayaraman, R.; Weiss, P. S.; Horn, M. W. *Microelectron. Eng.* **2005**, 78–79, 248–252. doi:10.1016/j.mee.2005.01.003
- Anderson, M. E.; Tan, L. P.; Tanaka, H.; Mihok, M.; Lee, H.; Horn, M. W.; Weiss, P. S. J. Vac. Sci. Technol., B 2003, 21, 3116–3119. doi:10.1116/1.1621662
- Srinivasan, C.; Anderson, M. E.; Carter, E. M.; Hohman, J. N.;
   Bharadwaja, S. S. N.; Trolier-McKinstry, S.; Weiss, P. S.; Horn, M. W.
   J. Vac. Sci. Technol., B 2006, 24, 3200–3204. doi:10.1116/1.2393252
- Srinivasan, C.; Hohman, J. N.; Anderson, M. E.; Weiss, P. S.; Horn, M. W. J. Vac. Sci. Technol., B 2007, 25, 1985–1988. doi:10.1116/1.2811712
- 21. Srinivasan, C.; Hohman, J. N.; Anderson, M. E.; Weiss, P. S.; Horn, M. W. Appl. Phys. Lett. 2008, 93, 083123. doi:10.1063/1.2963982
- Tanaka, H.; Anderson, M. E.; Horn, M. W.; Weiss, P. S. Jpn. J. Appl. Phys., Part 2 2004, 43, L950–L953. doi:10.1143/JJAP.43.L950
- 23. McCarty, G. S. Nano Lett. 2004, 4, 1391–1394. doi:10.1021/nl049375z
- Li, C. B.; Hasegawa, T.; Tanaka, H.; Miyazaki, H.; Odaka, S.;
   Tsukagoshi, K.; Aono, M. Nanotechnology 2010, 21, 495304.
   doi:10.1088/0957-4484/21/49/495304
- Anderson, M. E.; Mihok, M.; Tanaka, H.; Tan, L. P.; Horn, M. W.; McCarty, G. S.; Weiss, P. S. Adv. Mater. 2006, 18, 1020–1022. doi:10.1002/adma.200600108
- 26. McCarty, G. S.; Moody, B.; Zachek, M. K. J. Electroanal. Chem. 2010, 643, 9–14. doi:10.1016/j.jelechem.2010.03.018
- Daniel, T. A.; Uppili, S.; McCarty, G.; Allara, D. L. Langmuir 2007, 23, 638–648. doi:10.1021/la0621719
- Benson, A. S.; Elinski, M. B.; Ohnsorg, M. L.; Beaudoin, C. K.; Alexander, K. A.; Peaslee, G. F.; DeYoung, P. A.; Anderson, M. E. *Thin Solid Films* **2015**, *590*, 103–110. doi:10.1016/j.tsf.2015.07.048
- Johnson, S.; Chan, J.; Evans, D.; Davies, A. G.; Wälti, C. Langmuir
   2011, 27, 1033–1037. doi:10.1021/la103733j
- Evans, S. D.; Ulman, A.; Goppert-Berarducci, K. E.; Gerenser, L. J. J. Am. Chem. Soc. 1991, 113, 5866–5868. doi:10.1021/ja00015a053
- 31. Freeman, T. L.; Evans, S. D.; Ulman, A. *Thin Solid Films* **1994**, *244*, 784–788. doi:10.1016/0040-6090(94)90571-1
- Drexler, C. I.; Moore, K. B., III; Causey, C. P.; Mullen, T. J. Langmuir
   2014, 30, 7447–7455. doi:10.1021/la501645w
- 33. Kim, Y. T.; McCarley, R. L.; Bard, A. J. Langmuir 1993, 9, 1941–1944. doi:10.1021/la00032a001
- Woodward, J. T.; Walker, M. L.; Meuse, C. W.; Vanderah, D. J.;
   Poirier, G. E.; Plant, A. L. *Langmuir* 2000, *16*, 5347–5353.
   doi:10.1021/la991672+

## License and Terms

This is an Open Access article under the terms of the Creative Commons Attribution License (<a href="http://creativecommons.org/licenses/by/4.0">http://creativecommons.org/licenses/by/4.0</a>), which permits unrestricted use, distribution, and reproduction in any medium, provided the original work is properly cited.

The license is subject to the *Beilstein Journal of Nanotechnology* terms and conditions: (http://www.beilstein-journals.org/bjnano)

The definitive version of this article is the electronic one which can be found at:

doi:10.3762/bjnano.8.233

# **Supporting Information**

for

Expanding the molecular-ruler process through vapor deposition of hexadecanethiol

Alexandra M. Patron<sup>1</sup>, Timothy S. Hooker<sup>2</sup>, Daniel F. Santavicca<sup>2</sup>, Corey P. Causey\*\*,§,1 and Thomas J. Mullen\*\*,¶,1

Address: <sup>1</sup>Department of Chemistry, University of North Florida, Jacksonville, FL 32224, USA and <sup>2</sup>Department of Physics, University of North Florida, Jacksonville, FL 32224, USA

Email: Corey P. Causey\* - corey.causey@unf.edu; Thomas J. Mullen\* - tj.mullen@unf.edu

\*Corresponding author

§Phone: +1 904 620 2098; Fax: +1 904 620 3535

¶Phone: +1 904 620 1377; Fax: +1 904 620 3535

# **Additional AFM data**

Figures S1 shows a representative 500 nm  $\times$  500 nm AFM image of a Cu-ligated MHDA-C16 bilayer formed from the solution deposition of MHDA for 18 h, Cu(ClO<sub>4</sub>)<sub>2</sub>·6H<sub>2</sub>O for 5 min, and C16 for 1 h at 80°C. Islands of various apparent heights with relatively low surface coverages (46.8  $\pm$  2.9%) are observed. This surface morphology results in a RMS roughness of  $3.8 \pm 0.2$  nm.

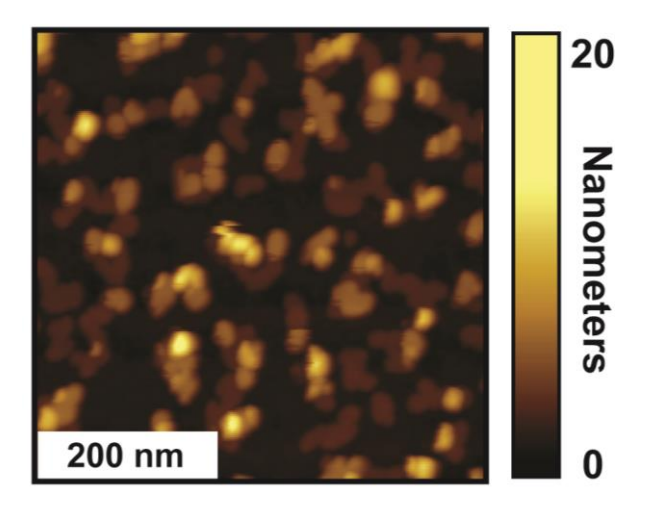


**Figure S1:** Cu-ligated MHDA-C16 bilayer formed from solution-phase deposition at 80 °C. Representative 500 nm  $\times$  500 nm AFM images of a Cu-ligated MHDA-C16 bilayer formed from the solution deposition of MHDA for 18 h, Cu(ClO<sub>4</sub>)<sub>2</sub>·6H<sub>2</sub>O for 5 min, and C16 for 1 h at 80 °C.

Figure S2A shows a representative 500 nm  $\times$  500 nm AFM image of a Cu-ligated MHDA-C16 multilayer formed from nine iterations of the solution deposition of MHDA and Cu(ClO<sub>4</sub>)<sub>2</sub>·6H<sub>2</sub>O followed by the solution deposition of MHDA for 1 h. Figure S2B displays a representative cursor profile as indicated by the red line in Figure S2A. The surface morphology results in a RMS roughness of  $1.4 \pm 0.1$  nm. Additionally, isolated protruding features are observed across the substrate. These features have been observed previously and are attributed to the dimerization and agglomeration of MHDA molecules [1]. Figures S2C shows a representative 500 nm  $\times$  500 nm AFM image of a Cu-ligated MHDA multilayer formed from ten iterations of the solution

deposition of MHDA and  $\text{Cu}(\text{ClO}_4)_2 \cdot 6\text{H}_2\text{O}$  followed by the vapor deposition of C16 at 80 °C for 1 h. Figure S2D displays a representative cursor profile as indicated by the red line in Figure S2C. The surface morphology results in a RMS roughness of  $1.7 \pm 0.1$  nm. Isolated protruding features, with similar heights and larger cross sections when compared to the MHDA multilayers without the C16 capping layer, are observed across the substrate. These features are attributed to the C16 molecules depositing across the entire substrate including the dimerized and agglomerated MHDA molecules.

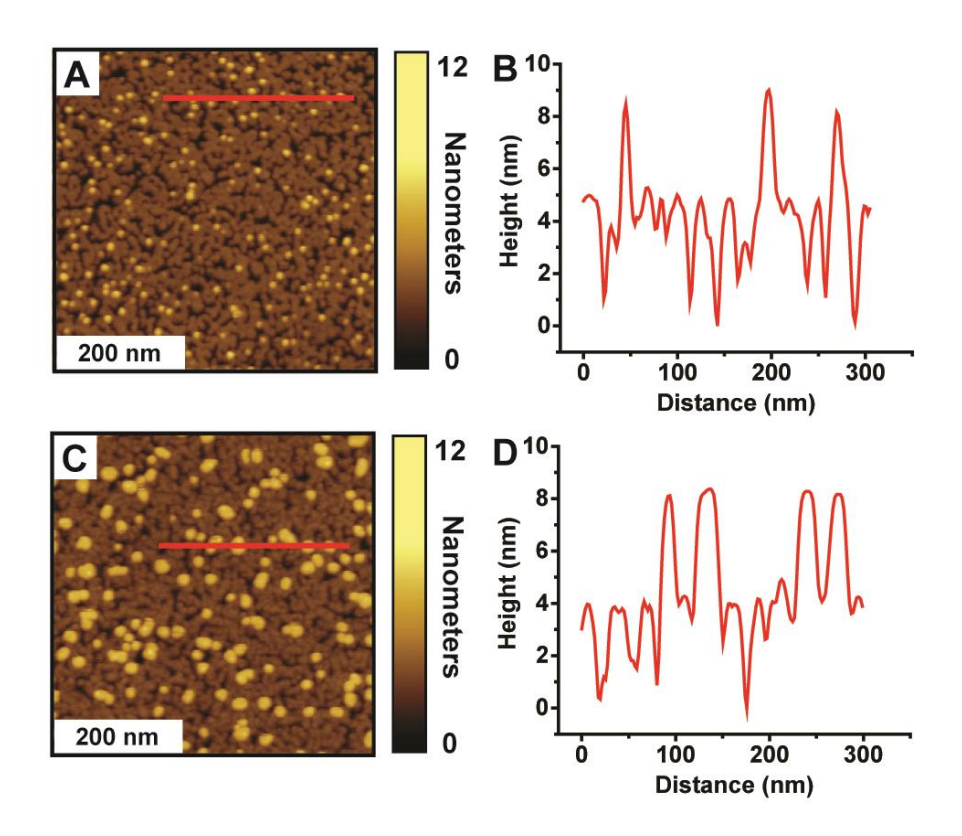


**Figure S2:** Cu-ligated MHDA multilayers from MHDA only and MHDA with vapor-phase deposition of C16. (A) A representative AFM image and (B) corresponding cursor profile of a Cu-ligated MHDA multilayer fabricated from nine iterations of the solution deposition of MHDA and  $\text{Cu}(\text{ClO}_4)_2 \cdot 6\text{H}_2\text{O}$  followed by the solution deposition of MHDA for 1 h. (C) A representative AFM image and (D) corresponding cursor profile of a Cu-ligated MHDA multilayer from ten iterations of the solution deposition of MHDA and  $\text{Cu}(\text{ClO}_4)_2 \cdot 6\text{H}_2\text{O}$  followed by the vapor deposition of C16 at 80 °C for 1 h.

# **Experimental details**

# Reagents and materials

16-Mercaptohexadecanoic acid (MHDA, 90%), 1-hexadecanethiol (C16, 95%), copper(II) perchlorate hexahydrate (Cu(ClO<sub>4</sub>)<sub>2</sub>·6H<sub>2</sub>O, 98%), and acetic acid (>99%) were purchased from Sigma-Aldrich (St. Louis, MO, USA). Nitric acid (ACS grade), hydrogen peroxide (30% aqueous solution), and sulfuric acid (ACS Grade) were purchased from VWR International (Randor, PA, USA). Absolute ethanol was purchased from Pharmco-Aaper (Bookfield, CT, USA). LOR-2A and Shipley 1813 photoresists, MF-319 developer, and Remover PG were purchased from MicroChem (Westborough, MA, USA). ACT-935 was purchased from Air Products (Allentown, PA, USA). All reagents were used as received. Water (18 M $\Omega$ ) was generated using a Milli-Q system (Q-GARD 2, Millipore, Billerica, MA, USA). Au wire (99.99%, 1 mm diameter) was purchased from Scientific Instrument Services (Ringoes, NJ, USA). Pt-Ir foil (99.9%, 0.1 mm thick) was purchased from Alfa Aesar (Tewksbury, MA, USA). Undoped 2-inch silicon wafers were purchased from University Wafer (South Boston, MA, USA). All glassware was cleaned by immersing in piranha solution (3:1 by volume of sulfuric acid/30% hydrogen peroxide) for 1 h, rinsing with copious amounts of 18 M $\Omega$  water, and drying overnight in ambient. Caution: piranha solution is a vigorous oxidant and should be used with extreme care!

# Preparation of Au substrates

For AFM experiments, Au beads with single crystal {111} facets were formed by melting Au wires mounted to Pt–Ir foils. Subsequently, the Au beads were positioned such that the single crystal {111} facets were parallel to the Pt–Ir foil [2-4]. The Au beads were cleaned by

immersing in hot (130 °C) nitric acid for 1 h, rinsed with copious amounts of 18 M $\Omega$  water, and dried under a stream of N<sub>2</sub>. Au beads were annealed with a H<sub>2</sub> flame for 20–30 s just prior to immersion into thiol solutions.

For the spectroscopic ellipsometry and nanofabrication experiments, Au thin film structures were patterned on Si substrates using a bilayer resist process. A bilayer resist was employed to ensure a clean edge on the patterned Au structure. First, a 2" Si wafer was spin-coated with LOR-2A photoresist and baked on a hotplate at 180 °C for 5 min. After cooling, it was spincoated with Shipley 1813 photoresist and baked on a hotplate for 2 min. at 100 °C. Photolithographic patterning was performed using a Karl-Suss MA4 mask aligner with a UV exposure time of 25 s followed by submersion in MF-319 developer for 180 s. Following development, the wafer was rinsed in 18 M $\Omega$  water and dried under a stream of N<sub>2</sub>. The wafer was then loaded into a thermal deposition system. After reaching a pressure of less than  $10^{-6}$  Torr, 4 nm of Cr was deposited as an adhesion layer, followed by the deposition of 100 nm of Au. Lift-off was performed by soaking in Remover PG at 70 °C for 1 h followed by 5 min of sonication. The patterned wafers were then diced into four 1 cm × 3 cm chips. Each chip was cleaned by immersing in piranha solution for 30 min, rinsed with copious amounts of 18 M $\Omega$ water, dried under a stream of N<sub>2</sub>. Subsequently, the chip was cleaned using a UV ozone cleaner (Novascan, PSDP-UVT, Ames, IA, USA) for 30 min, rinsed with absolute ethanol, and dried under a stream of  $N_2$  prior to immersion into thiol solutions.

# Preparation of Cu-ligated multilayers and nanogaps

Au substrates were immersed into 0.1 mM MHDA ethanoic solutions with 1.5 M acetic acid for 18–24 h. Acetic acid helps suppress the dimerization and agglomeration of the MHDA molecules

by competing for hydrogen-bonding interactions [1,5-7]. Subsequently, the Au substrates with the MHDA SAMs were rinsed with absolute ethanol, immersed into 5 mM Cu(ClO<sub>4</sub>)<sub>2</sub>·6H<sub>2</sub>O ethanolic solutions for 5 min, and rinsed with absolute ethanol. To grow multilayers of MHDA, the Au substrates were immersed into 1 mM ethanolic solutions of MHDA for 1 h and rinsed with absolute ethanol. This sequence of immersion into ethanolic solutions of Cu(ClO<sub>4</sub>)<sub>2</sub>·6H<sub>2</sub>O and MHDA was repeated until the number of desired layers was achieved. It is important to note that only the initial MHDA monolayer in Cu-ligated MHDA multilayers was assembled from a 0.1 mM MHDA ethanolic solution with 1.5 M acetic acid; the subsequent layers of the multilayers were assembled from 1 mM MHDA ethanolic solutions without acetic acid. We observed that 0.1 mM MHDA ethanolic solutions with 1.5 M acetic acid disrupt the assembly of the Cu-ligated MHDA multilayers and typically resulted in MHDA monolayers.

Two methods for the deposition, solution and vapor, of a terminal layer of C16 were explored. To deposit a C16 layer from solution, Au substrates with MHDA monolayers and/or multilayers were immersed into 5 mM Cu(ClO<sub>4</sub>)<sub>2</sub>·6H<sub>2</sub>O ethanolic solutions for 5 min, rinsed with absolute ethanol, and into 1 mM C16 ethanolic solutions for 1 h. The Au substrates were subsequently rinsed with absolute ethanol and dried under a stream of N<sub>2</sub>. To deposit a C16 layer from vapor, Au substrates with MHDA monolayers and/or multilayers were immersed into 5 mM Cu(ClO<sub>4</sub>)<sub>2</sub>·6H<sub>2</sub>O ethanolic solutions for 5 min and rinsed with absolute ethanol. Approximately, 1 mL of neat C16 was pipetted into a 10 mL beaker. The Au substrates and the 10 mL beaker were then placed into a glass jar and sealed. The glass jar was held at 80 °C for 1 h, exposing the Au substrate to vapor-phase C16. The Au substrates were removed from the glass jar, rinsed with absolute ethanol, and dried under a stream of N<sub>2</sub>. All SAMs and multilayers were imaged or utilized for hybrid-nanolithography immediately after preparation.

For the molecular-ruler process, samples were returned to the thermal deposition system. 3 nm of Cr was deposited followed by 30 nm of Au. Following deposition, the multilayer is removed by soaking the sample in ACT-935 at 75  $^{\circ}$ C for 1 h followed by 5 min of sonication. The sample is then rinsed in absolute ethanol and dried under a stream of  $N_2$ .

## **Atomic force microscopy**

Tapping-mode (AC-mode) atomic force microscopy (AFM) images were acquired using an Agilent 5420 scanning probe microscope with OLTESPA Si cantilevers (Bruker AFM probes, Santa Barbra, CA, USA) with nominal force constants of 2 N/m. The Si cantilevers were cleaned using a UV/ozone cleaner (Novascan, PSDP-UVT, Ames, IA, USA) for 20 min to remove surface contaminants [8]. The drive frequency of the cantilever was offset by 0.1 kHz lower than the cantilever resonance to maintain repulsive probe-surface interactions [9,10]. The damping of the amplitude was set at 60–70% of free oscillation, and scan rates were set to 2.00 Hz. All AFM images were acquired at 256 points per line under ambient conditions. Image processing and analysis of the AFM images were performed using Gwyddion (version 2.48, "Magnetic Monastery"), which is an open-source software freely available on the internet and supported by the Czech Metrology Institute [11].

The AFM images used for analysis were acquired from several regions across each type of Cu-ligated multilayer, and the resulting apparent heights, surface coverages, and RMS roughnesses were averaged. The average and standard deviation (average  $\pm$  standard deviation) of the apparent heights of the various features of the Cu-ligated multilayers were determined from cursor profiles from 500 nm  $\times$  500 nm AFM images across at least 30 features. The average and standard deviation (average  $\pm$  standard deviation) of the surface coverages of the C16 islands

in the of Cu-ligated multilayers were calculated by counting the number of pixels above a thickness threshold and dividing by the total number of pixels in a set of at least four 500 nm  $\times$  500 nm AFM images for each type of multilayer. The thickness threshold values were determined by using the full-width-at-half-height across several protruding islands of C16 within the AFM images [12-18]. The average and standard deviation (average  $\pm$  standard deviation) of the RMS roughnesses of the Cu-ligated multilayers were calculated using a set of at least four 500 nm  $\times$  500nm AFM images for each type of multilayer.

## **Spectroscopic ellipsometry**

Spectroscopic ellipsometry measurements were acquired using a rotating compensator spectroscopic ellipsometer (Alpha-SE, J.A. Woollam Inc.) where 180 wavelengths between 380–900 nm were measured at a fixed  $70^{\circ}$  angle of incidence The Cu-ligated multilayer thicknesses were calculated using the CompleteEASE software package; a B-spline model was used for the Au substrate, and a Cauchy model was used for the multilayer film using a refractive index value of n = 1.5 [19-21]. Measurements were collected on multiple regions across each type of Cu-ligated multilayer, and the average and standard deviation (average  $\pm$  standard deviation) of the resulting calculated thicknesses were determined.

### **Scanning electron microscopy**

Scanning electron microscopy (SEM) images of the molecular-ruler samples were acquired using a TESCAN MIRA field-emission SEM. The size of the nanogap was determined by taking approximately 10 images at a magnification of  $2 \times 10^5$  at various locations on each sample. On each image, the pixel intensity as a function of position was plotted for multiple linescans taken

perpendicular to the nanogap. A numerical procedure developed in the software program Igor Pro was used to determine the gap width by finding the full-width-at-half-minimum of each linescan. A total of 100 linescans for each sample (both without and with the C16 capping layer) were used to calculate the average and standard deviation (average ± standard deviation) of the nanogap width.

## References

- 1. Drexler, C. I.; Moore, K. B.; Causey, C. P.; Mullen, T. J. *Langmuir* **2014**, *30*, 7447-7455.
- 2. Shao, J.; Josephs, E. A.; Lee, C.; Lopez, A.; Ye, T. ACS Nano 2013, 7, 5421-5429.
- 3. Josephs, E. A.; Ye, T. J. Am. Chem. Soc. **2012**, 134, 10021-10030.
- 4. Calavilier, J.; Faure, R.; Guinet, G.; Durand, R. *J. Electroanal. Chem.* **1980**, *107*, 205-209.
- 5. Lee, C.; Josephs, E. A.; Shao, J.; Ye, T. *J. Phys. Chem. C* **2012**, *116*, 17625-17632.
- 6. Snow, A. W.; Jernigan, G. G.; Ancona, M. G. Analyst 2011, 136, 4935-4949.
- 7. Kelley, A. T.; Ngunjiri, J. N.; Serem, W. K.; Lawrence, S. O.; Yu, J.-J.; Crowe, W. E.; Garno, J. C. *Langmuir* **2010**, *26*, 3040-3049.
- 8. Lo, Y. S.; Huefner, N. D.; Chan, W. S.; Dryden, P.; Hagenhoff, B.; Beebe, T. P. Langmuir 1999, 15, 6522-6526.
- 9. Garcia, R.; Perez, R. Surf. Sci. Rep. 2002, 47, 197-301.
- 10. Weisenhorn, A. L.; Maivald, P.; Butt, H. J.; Hansma, P. K. *Phys. Rev. B* **1992**, *45*, 11226-11232.
- 11. Necas, D.; Klapetek, P. Cent. Eur. J. Phys. **2012**, 10, 181-188.
- 12. Drexler, C. I.; Causey, C. P.; Mullen, T. J. Scanning **2015**, *37*, 6-16.

- 13. Brownfield, A. L.; Causey, C. P.; Mullen, T. J. Thin Solid Films 2015, 594, 184-191.
- 14. Brownfield, A. L.; Causey, C. P.; Mullen, T. J. J. Phys. Chem. C 2015, 119, 12455-12463.
- 15. Bu, D. L.; Mullen, T. J.; Liu, G. Y. ACS Nano **2010**, *4*, 6863-6873.
- 16. Dameron, A. A.; Hampton, J. R.; Smith, R. K.; Mullen, T. J.; Gillmor, S. D.; Weiss, P. S. *Nano Lett.* **2005**, *5*, 1834-1837.
- 17. Mullen, T. J.; Dameron, A. A.; Saavedra, H. M.; Williams, M. E.; Weiss, P. S. *J. Phys. Chem. C* **2007**, *111*, 6740-6746.
- 18. Mullen, T. J.; Srinivasan, C.; Hohman, J. N.; Gillmor, S. D.; Shuster, M. J.; Horn, M. W.; Andrews, A. M.; Weiss, P. S. *Appl. Phys. Lett.* **2007**, *90*.
- 19. Evans, S. D.; Ulman, A.; Goppertberarducci, K. E.; Gerenser, L. J. *J. Am. Chem. Soc.* **1991**, *113*, 5866-5868.
- 20. Benson, A. S.; Elinski, M. B.; Ohnsorg, M. L.; Beaudoin, C. K.; Alexander, K. A.; Peaslee, G. F.; DeYoung, P. A.; Anderson, M. E. *Thin Solid Films* **2015**, *590*, 103-110.
- 21. Daniel, T. A.; Uppili, S.; McCarty, G.; Allara, D. L. Langmuir **2007**, *23*, 638-648.